C/SiC复合材料表面状态对其与Nb钎焊的影响

刘玉章，　张丽霞，　杨振文，　冯吉才*
(哈尔滨工业大学 现代焊接生产技术国家重点实验室，哈尔滨　150001)


刘玉章

摘　要：采用等原子比Ti-Ni复合箔对C/SiC复合材料与Nb进行了真空反应钎焊，研究了焊前C/SiC表面状态对接头界面组织和力学性能的影响. 结果表明，线切割态的C/SiC与Nb的接头界面(Ti, Nb)C反应层呈现锯齿状，而抛光和砂纸打磨状态的C/SiC接头界面处的反应层平直. 锯齿状的界面反应层降低了界面处的应力集中程度，有助于提高接头的力学性能，使得线切割态的C/SiC与Nb的接头强度明显高于抛光和打磨状态的接头，达到188 MPa. 线切割态的C/SiC与Nb的接头断裂同时发生在C/SiC母材、界面和钎缝中，而抛光和打磨状态的C/SiC与Nb的接头断裂主要发生在界面处.
关键词：C/SiC复合材料；钎焊；表面状态；组织；抗剪强度
中图分类号：TG454　　文献标识码：A　　文章编号：0253-360X(2010)10-0031-04

0　序　言

C/SiC复合材料是一种新型高温结构材料，具有轻质，耐高温和类金属断裂的特点，在航空航天、武器装备等领域具有广泛的应用前景. 但由于制备方法的限制难以获得复杂形状的构件，实现C/SiC与其它材料的可靠连接是其走向工程应用的关键.

目前国内外关于C/SiC的连接报道的方法有钎焊[1-5]、扩散连接[6]、液相渗透连接[7]、先驱体连接[8,9]等，其中钎焊接头的性能较好，对复杂结构也有较高的适应性. 但不同于均质材料，C/SiC由C纤维、SiC基体和孔洞组成，钎焊时需要同时考虑多个性质不同的表面. 经过切割/打磨的C/SiC表面状态更为复杂，这必然对连接产生较大的影响. 上述文献中，仅Asthana等人[3]在研究Ag-Cu-Ti钎焊C/SiC与Al_2O_3时发现，焊前对C/SiC表面进行抛光可以提高Ti元素在界面处的富集程度，有助于提高接头的质量. 其余文献并未对C/SiC表面状态对连接的影响进行过对比研究.

采用等原子比Ti-Ni复合箔对C/SiC与Nb进行真空反应钎焊，着重研究C/SiC的三种表面状态(线切割、抛光和砂纸打磨)对接头界面组织及力学性能的影响.

收稿日期：2010-02-08
基金项目：国家自然科学基金资助项目(50705022)
*参加此项工作的还有李宏伟

1　试验方法

C/SiC为采用先驱体聚碳硅烷浸渍裂解法(PIP)制备的三维四向复合材料. 试验前采用电火花线切割将C/SiC和Nb板分别切割成3 mm×5 mm×6 mm和3 mm×20 mm×30 mm试块. C/SiC的被焊表面状态及获得方法如表1所示. Nb板的被焊表面采用600号水砂纸磨平后超声波丙酮清洗.

表1　C/SiC复合材料的被焊表面状态
Table 1　Brazing surface state of C/SiC composites

表面状态	获得方法
线切割	线切割，超声波丙酮清洗
抛光	200～1 500号水砂纸逐级打磨，1 μm金刚石抛光
打磨	600号水砂纸打磨平整，超声波丙酮清洗

钎焊的原始中间层材料为纯度(质量分数，%)高于99.6%的厚度为80 μm Ti，100 μm Ti*和80 μm Ni箔. 焊前将箔片按照Ti/Ni/Ti*/Ni/Ti的方式复合并加工成面积为5 mm×6 mm的试块. 复合箔中Ti和Ni的原子比约为50∶50，简记为Ti50Ni50. 钎焊时，将材料按照从下到上Nb/Ti50Ni50/(C/SiC)的形式进行装配，然后放入真空炉中进行钎焊. 钎焊过程中真空度优于5×10^{-3} Pa，钎焊温度为1 180 ℃，保温时间为20 min，钎焊时的压力约为1 000 Pa.

采用电子万能试验机(Instron-5569)测试接

头的室温抗剪强度，强度值取5个试样的平均值．采用扫描电子显微镜（SEM，S—3400）观察C/SiC的表面状态，焊后接头的界面组织及断口形貌，用能谱分析仪（EDS）结合旋转阳极X射线衍射仪（XRD）分析接头的界面产物．

2 试验结果及分析

2.1 C/SiC复合材料的表面状态

图1为不同状态的C/SiC的表面形貌，可以看出，C纤维和SiC基体的凸凹程度有明显差别．线切割后C纤维凸出而SiC凹陷，抛光后表面平整，砂纸打磨后C纤维凹陷而SiC凸出．

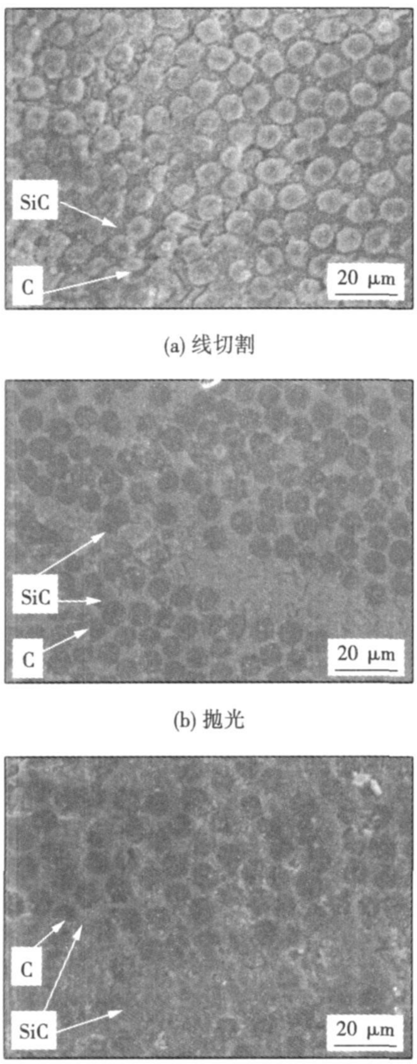

(a) 线切割

(b) 抛光

(c) 打磨

图1 C/SiC复合材料被焊表面形貌

Fig. 1 Brazing surface morphology of C/SiC composites

形貌的差别主要是C纤维和SiC基体性质的差异造成的。C纤维的熔点（>3 500 ℃）远高于SiC的分解温度（约2 700 ℃），因此线切割时电火花对SiC的烧蚀比C纤维严重，最终切割表面的C纤维凸出．而C纤维的硬度远低于SiC，打磨时C纤维的磨损比SiC严重，使得打磨后的表面C纤维凹陷．抛光是在砂纸逐级打磨后进行的，其主要是不断磨削C/SiC表面凸起的部分而使得表面逐渐平整．

焊接过程中被焊表面的凸起部分将首先和中间层材料接触，其与中间层材料的反应也更为充分，这必然影响最终接头的界面组织和力学性能．

2.2 C/SiC复合材料表面状态对接头界面的影响

图2为采用Ti50Ni50复合箔在1 180 ℃/20 min钎焊的不同状态的C/SiC与Nb的接头界面．表2为图2中各相的化学成分．图3为钎焊接头靠近C/SiC侧和焊缝中部的XRD分析结果（图2a中虚线箭头Ⅰ和Ⅱ所在垂直平面）．

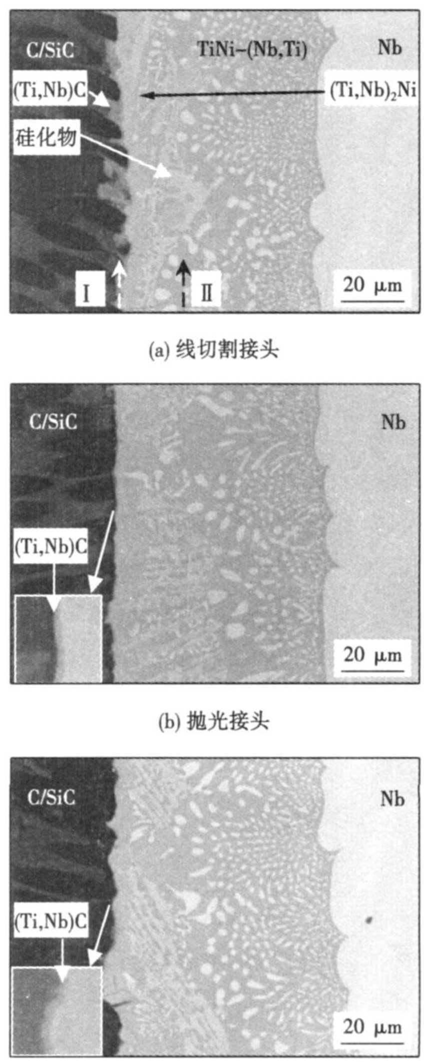

(a) 线切割接头

(b) 抛光接头

(c) 打磨接头

图2 Nb与不同表面状态C/SiC复合材料钎焊接头界面

Fig. 2 Microstructure of brazing joint of Nb and C/SiC at different surface state

表 2　图 2中各相的能谱分析结果(原子分数,%)
Table 2　EDS analysis of phases identified in Fig. 2

可能相	Nb	Ti	Ni	Si
TiNi	6~10	38~42	50~52	1
(Nb, Ti)	83~86	10~11	3~5	1~2
(Ti, Nb)C	19	77	2	2
$(Ti, Nb)_2Ni$	11~24	42~53	33~35	1~2
硅化物	44	24	24	8

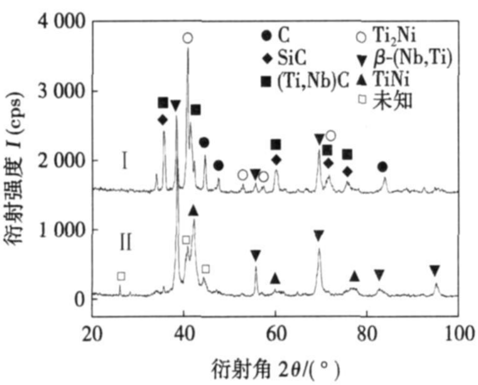

图 3　C/SiC复合材料与 Nb钎焊接头逐层 XRD分析结果
Fig. 3　XRD patterns of C/SiC composites and Nb brazing joint

从表 2可以看出焊缝中含有大量 Nb,表明钎焊过程中母材中的 Nb向钎料中溶解. 根据文献[10]的报道, TiNi和 Nb可以在 1 150.7 ℃形成共晶,而文中的焊接温度超过了该温度. 因此接头中出现了大量的 TiNi-(Nb, Ti)共晶组织,图 3的 XRD分析结果也证实了 TiNi和 (Nb, Ti)的存在. 结合图 2,图 3和表 2的结果,在 C/SiC侧界面处形成了 (Ti, Nb)C反应层. 紧挨 (Ti, Nb)C层的是灰色的 $(Ti, Nb)_2Ni$相,该相是间隙原子 C稳定 Ti_2Ni型晶格形成的,其饱和结构为 $(Ti, Nb)_4Ni_2(O, C)$[11]. 此外焊缝中还出现了含有较多 Si元素的白灰色四元相,该相的晶体结构参数未知,为表述方便下文称之为硅化物. 对比图 2a, b, c可以看出,不同表面状态下的接头界面相组成相同,但各相的相对含量和 C/SiC侧界面处的 (Ti, Nb)C层形貌有明显差别.

按照线切割、抛光、打磨的顺序,接头中硅化物的相对含量增多, TiNi-(Nb, Ti)共晶的相对含量减少. 反应相含量的变化与钎料和 C/SiC的界面反应有关. Ti和 Nb均为钎焊陶瓷的活性元素[12],均可以与 C/SiC发生反应. 其可能的反应如下:

$$(Ti, Nb) + C \rightarrow (Ti, Nb)C \qquad (1)$$

$$(Ti, Nb) + SiC \rightarrow (Ti, Nb)C + Si \qquad (2)$$

反应 (1)和 (2)的发生使 C/SiC侧界面处形成 (Ti, Nb)C反应层,反应 (2)会将 Si元素引入钎缝.

线切割状态下,与液态钎料接触的 C纤维面积比打磨状态下大,与钎料接触的 SiC的面积比打磨状态下小,因此虽处于相同的钎焊条件,线切割状态下的反应 (1)强于打磨状态,而反应 (2)弱于打磨状态. 使得打磨状态下,由反应 (2)引入钎缝的 Si元素的总量大于线切割状态,最终接头中的硅化物的量比线切割状态多. 抛光状态的接头介于二者之间,更接近打磨状态.

焊前线切割状态的 C/SiC表面 C纤维凸出, SiC凹陷,而钎料与 C/SiC界面反应形成的 (Ti, Nb)C在 C/SiC表面析出长大,最终形成了锯齿状. 相比于抛光和打磨状态下平直的界面 (Ti, Nb)C反应层,锯齿状的 (Ti, Nb)C层使得从 C/SiC母材到焊缝的过渡区域范围扩大,过渡更为平缓,降低了界面处的应力集中程度,对接头的性能有利.

2.3　C/SiC复合材料表面状态对接头性能的影响

焊后接头的室温抗剪强度测试结果表明,线切割状态下的接头强度最高,达到 188 MPa,而抛光和打磨状态下的接头强度分别只有 151和 142 MPa.

接头的强度受到界面结合和残余应力分布的影响,承载时接头的断裂位置是接头薄弱环节的反映. 图 4为不同表面状态下的 C/SiC与 Nb的接头剪切断口 (Nb侧)典型区域的形貌.

从图 4可以看出,线切割状态下,断裂主要发生

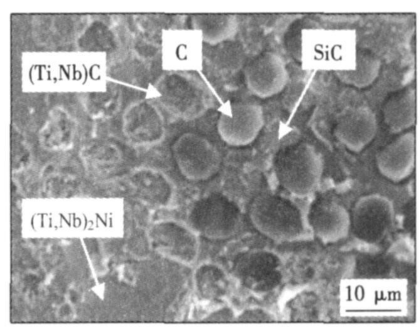

(a) 线切割断口

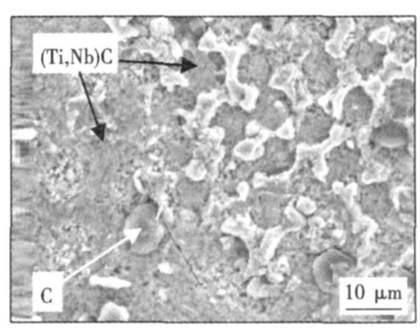

(b) 抛光断口

图 4　C/SiC与 Nb钎焊接头剪切断口典型形貌
Fig. 4　Fracture surface morphology of C/SiC and Nb brazing joints after shear test

在近缝区的 C/SiC母材,(Ti,Nb)C反应层与 C/SiC的界面以及钎缝中的(Ti,Nb)$_2$N相. 断裂的 C/SiC母材出现了纤维的脱粘和拨出,呈现一定的伪塑性.(Ti,Nb)$_2$N相的断口光滑,为解理断裂. 抛光状态下,断裂主要发生在(Ti,Nb)C反应层与 C/SiC的界面处,另外有少量 C纤维被剪断而留在了断口表面. 打磨状态下的断裂方式与抛光状态下的基本相同,主要断裂于界面处.

在相同的钎焊工艺下,钎料与 C/SiC的界面结合情况类似,相对于锯齿形的界面反应层,平直的界面反应层处残余应力集中程度较高,容易成为接头的薄弱环节,承载时,裂纹几乎完全沿着平直界面扩展直至断裂.

3 结 论

(1)经过线切割、抛光、打磨后的 C/SiC复合材料表面形貌不同. 线切割后的 C/SiC表面 C纤维凸出, SiC凹陷;抛光后的 C/SiC表面基本平整;而打磨后的 C/SiC表面 C纤维凹陷, SiC凸出.

(2)相同工艺钎焊时,线切割状态的 C/SiC与 Nb的接头界面(Ti,Nb)C反应层呈现锯齿状;而打磨和抛光状态下的接头界面(Ti,Nb)C层平直.

(3)相对于平直的(Ti,Nb)C界面反应层,线切割状态下锯齿状的(Ti,Nb)C层扩大了 C/SiC向钎料的过渡范围,降低了界面处的残余应力集中程度,对接头强度有利. 使得 C/SiC与 Nb的接头强度最高,室温抗剪强度达到 188 MPa,剪切断裂同时发生在 C/SiC母材、(Ti,Nb)C反应层和钎缝.

参考文献:

[1] Lin G B, Huang J H. Brazed joints of C_f/SiC composite to Ti alloy using Ag-Cu-Ti-(Ti+C) mixed powder as interlayer[J]. Powder Metallurgy, 2006, 49(4): 345−348.

[2] Lin G B, Huang J H, Zhang H. Joints of carbon fiber-reinforced SiC composites to Ti-alloy brazed by Ag-Cu-Ti short carbon fibers[J]. Journal of Materials Processing Technology, 2007, 189(1−3): 256−261.

[3] Asthana R, Singh M. Joining of partially sintered alumina to alumina, titanium, Hastealloy and C-SiC composite using Ag-Cu brazes[J]. Journal of the European Ceramic Society, 2008, 28(3): 617−631.

[4] Singh M, Asthana R, Shpargel T P. Brazing of ceramic-matrix composites to Ti and Hastealloy using Ni-base metallic glass interlayers[J]. Materials Science and Engineering A, 2008, 498: 19−30.

[5] Salvo M, Ferraris M, Lemoine P, et al. Joining of CMCs for thermonuclear fusion application[J]. Journal of Nuclear Materials, 1996, 233−237: 947−953.

[6] Xiong J T, Li J L, Zhang F S, et al. Joining of 3D C/SiC composites to niobium alloy[J]. Scripta Materialia, 2006, 55(2): 151−154.

[7] 童巧英, 成来飞, 张立同. 三维 C/SiC复合材料在线液相渗透连接[J]. 稀有金属材料与工程, 2004, 33(1): 101−104.
Tong Qiaoying, Cheng Laifei, Zhang Litong. On-line joining of 3D fiber reinforced C/SiC composites[J]. Rare Metal Materials and Engineering, 2004, 33(1): 101−104.

[8] Liu H L, Li S J, Chen Z J. Joining of C_f/SiC ceramic matrix composite using SiC-Si_3N_4 preceramic polymer[J]. Materials Science Forum, 2005, 475−479: 1267−1270.

[9] 所 俊, 陈朝辉, 韩卫敏, 等. 硅树脂高温转化陶瓷结合层连接陶瓷材料[J]. 硅酸盐学报, 2005, 33(3): 386−390.
Suo Jun, Chen Zhaohui, Han Weimin, et al. Joining of ceramic materials by ceramic bonding transformed from silicone resin at high temperature[J]. Journal of the Chinese Ceramic Society, 2005, 33(3): 386−390.

[10] Piao M, Otsuka K, Miyazaki S, et al. Effects of Nb addition on the microstructure of Ti-Ni alloys[J]. Materials Transactions, JIM, 1992, 30(4): 337−345.

[11] Zheng H X, Mentz J, Bram M, et al. Powder metallurgical production of TiNiNb and TiNiCu shape memory alloys by combination of pre-alloyed and elemental powders[J]. Journal of Alloys and Compounds, 2008, 463: 250−256.

[12] Lee H J, Lee J Y. A study of the wetting, microstructure and bond strength in brazing SiC by Cu-X(X=Ti, V, Nb, Cr) alloys[J]. Journal of Materials Science, 1996, 31(8): 4133−4140.

作者简介: 刘玉章, 男, 1982年出生, 博士研究生. 主要从事复合材料的连接研究. 发表论文 2篇.

Email: lyuzhang163@163.com

(1. School of Material Science and Engineering, Jiangsu University, Zhenjiang 212013, China; 2. State Key Laboratory of Advanced Welding Production Technology, Harbin Institute of Technology, Harbin 150001, China). p 17—21

Abstract: The SiC_p/6061Al MMCs joints were produced by arc-ultrasonic plasma arc in-situ weld-alloying by argon-nitrogen mixture as plasma gases and Ti wire as filler composite, and the effect of arc-ultrasonic on the microstructures and mechanical properties of the joints was investigated. The results indicate that without arc-ultrasonic (conventional plasma arc welding (PAW)), new phase AlN is slender needle-like, Al_3Ti is bulky, and the new particles such as TiC and TiN distribute unevenly in weld. Because arc-ultrasonic can refine the new reinforced composites such as TiC and TiN significantly and improve their distribution, new phase Al_3Ti become smaller and less. The test results of mechanical property show that the maximum tensile strength of the welded joint gained with arc-ultrasonic is 225 MPa, raising about 7% compared with conventional PAW.

Key words: SiC_p/Al MMCs; plasma arc welding; arc-ultrasonic; mechanical property

Finite element analysis of residual stress in weld and bolt beam-column connections YU Jiahuan, DAI Li, LI Hongshuang, LIU Qiongyang (School of Civil Engineering, Shenyang Jianzhu University, Shenyang 110168, China). p 22—26

Abstract: Three dimensional finite element model of welding beam-column connection components, including angle steel, bolt, beam and column, is established by taking account of the effect of temperature on the thermo-physical properties and mechanical properties of metal, and the temperature and the residual stress distributions during heating and cooling process are accurately computed by using of ANSYS software. The results show that the welding region is dominated mainly by tensile stress and different components possess different residual stress value. The maximum and minimum residual stresses occur in the bolts, which are 220.8% and 11.45% of the designing strength value respectively and are in accord with 'Code of Steel Structure'.

Key words: composite connection; welding; bolt; residual stress

Simulation of solidification microstructure in welded molten pool of nickel-based alloy DONG Zhibo[1], MA Rui[1], WANG Yong[1], ZHAN Xiaohong[1], WEI Yanhong[1,3] (1. State Key Laboratory of Advanced Welding Production Technology, Harbin Institute of Technology, Harbin 150001, China; 2. Shanghai Xinli Institute of Power Equipment, Shanghai 200125, China; 3. School of Material Science and Technology, Nanjing University of Aeronautics & Astronautics, Nanjing 210016, China). p 27—30

Abstract: Original cellular automaton capture rule was modified and applied to simulate dendrite growth during solidification process in welded molten pool of nickel-based alloy. The results show that the competitive growth between dendrites with different crystallographic axes orientations is intense. The grains whose crystallographic axes orientations are in accordance with the direction of largest temperature gradient have a fast growth speed and overgrow other grains, so that they can keep growing during solidification process. Meanwhile, solute concentrates in the residual liquid in the closed zone among dendrites and dendrite arms, which can lead to severe grain-boundary segregation after solidification process.

Key words: welded molten pool; dendrite growth; epitaxial growth; cellular automaton

Effects of surface state of C/SiC composites on brazing of C/SiC to Nb LIU Yuzhang, ZHANG Lixia, YANG Zhenwen, FENG Jicai, LI Hongwei (State Key Laboratory of Advanced Welding Production Technology, Harbin Institute of Technology, Harbin 150001, China). p 31—34

Abstract: C/SiC composites and Nb were brazed with equiatomic ratio TiNi composite foils in vacuum, and the effects of surface state of C/SiC composites on the microstructure and property of the brazing joints were investigated. The results showed that the (Ti,Nb)C reaction layer between C/SiC and filler metal in the brazing joint was serrate when the C/SiC surface state was cut by the electric spark linear cutting machine, but the (Ti,Nb)C layers were both flat when the surface of C/SiC were polished and sanded before brazing. The serrate reaction layer decreased the stress concentration at the C/SiC-filler metal interface and was benefit for the joint. The shear strength of brazing joints of Nb and C/SiC at spark cutting state reached 188 MPa, which is much higher than that at polishing and sanding states. The fracture of brazing joints of Nb and C/SiC at spark cutting state took place at C/SiC base material, C/SiC-filler metal interface and filler metal, but that of the other two kinds of joints mainly occurred at the C/SiC-filler metal interface.

Key words: C/SiC composites; braze; surface state; microstructure; shear strength

Mechanism investigation of Bi layer formation at anode interface in Cu/Sn-58Bi/Cu solder joint induced by electromigration HE Hongwen[1,2], XU Guangchen[1], GUO Fu[1] (1. College of Material Science and Engineering, Beijing University of Technology, Beijing 100124, China; 2. Department of Mechanical Engineering, Tsinghua University, Beijing 100084, China). p 35—38, 42

Abstract: Mechanism of Bi layer formation at the anode interface in Cu/Sn-58Bi/Cu solder joint was investigated under current density of 5×10^3 to 1.2×10^4 A/cm^2. During electromigration process, Bi was the main diffusing species which migrated from the cathode side to the anode side under electromigration force. Bi was the first species to reach anode interface because the diffusion velocity of Bi is faster than that of Sn. Therefore, compressive stress was formed at the anode interface when much more Bi atoms accumulated there and compelled Sn to migrate towards the cathode side, and the continuous Bi layer was formed at the anode interface. In the mean time, tensile stress was formed at the cathode interface due to the departure of metal atoms, which led to voids and cracks formation. The morphology of the Bi layer included planar-type layer and groove-type layer. The diffusing channels of the Bi atoms were Bi grain boundaries, Sn grain boundaries and Sn/Bi interfaces. With the current density and stressing time increasing, the Bi layer thickness increased. The electromigration force and Joule heating took on the